Cell

Nuclear Size Is Regulated by Importin α and Ntf2 in *Xenopus*

Daniel L. Levy[1] and Rebecca Heald[1,*]
[1]Department of Molecular and Cell Biology, University of California, Berkeley, Berkeley, CA 94720-3200, USA
*Correspondence: bheald@berkeley.edu
DOI 10.1016/j.cell.2010.09.012

SUMMARY

The size of the nucleus varies among different cell types, species, and disease states, but mechanisms of nuclear size regulation are poorly understood. We investigated nuclear scaling in the pseudotetraploid frog *Xenopus laevis* and its smaller diploid relative *Xenopus tropicalis*, which contains smaller cells and nuclei. Nuclear scaling was recapitulated in vitro using egg extracts, demonstrating that titratable cytoplasmic factors determine nuclear size to a greater extent than DNA content. Nuclear import rates correlated with nuclear size, and varying the concentrations of two transport factors, importin α and Ntf2, was sufficient to account for nuclear scaling between the two species. Both factors modulated lamin B3 import, with importin α increasing overall import rates and Ntf2 reducing import based on cargo size. Importin α also contributes to nuclear size changes during early *X. laevis* development. Thus, nuclear transport mechanisms are physiological regulators of both interspecies and developmental nuclear scaling.

INTRODUCTION

Cell size varies widely among different organisms, as well as within the same organism in different tissue types and during development, placing variable metabolic and functional demands on internal organelles (Hall et al., 2004). A fundamental question in cell biology is how organelle size is regulated to accommodate cell size differences. Models proposed to describe the regulation of organelle size can be broadly divided into those involving static mechanisms, in which the amount or size of one structural component determines the organelle's size, or dynamic mechanisms whereby feedback from the organelle regulates its own assembly or balances rates of assembly and disassembly (Marshall, 2002, 2008). Although these models have been applied to size control of relatively simple linear structures like flagella (Wilson et al., 2008) and stereocilia (Manor and Kachar, 2008), mechanisms that regulate the size of organelles with more complex geometries have been difficult to elucidate.

The nucleus is a particularly important example of an organelle that exhibits wide variations in size among eukaryotes, with nuclear surface area spanning over two orders of magnitude from budding yeast to certain amphibians (Maul and Deaven, 1977). Although correlations between ploidy and the size of the nucleus are well documented (Cavalier-Smith, 2005; Fankhauser, 1939), when genetic and growth conditions were altered in budding and fission yeasts, nuclear size varied with cell size and not ploidy (Jorgensen et al., 2007; Neumann and Nurse, 2007). The functional significance of maintaining proper nuclear morphology is unclear, but defects in nuclear size and shape are associated with and diagnostic of human disease, including cancer and other pathologies (Webster et al., 2009; Zink et al., 2004).

Whereas molecular mechanisms that determine nuclear size are largely unknown, structural components of the nucleus likely play a role. In metazoans, the nuclear envelope (NE) is composed of a double lipid bilayer perforated by nuclear pore complexes (NPCs) that mediate nucleocytoplasmic transport. The outer NE is continuous with the endoplasmic reticulum (ER), and the inner NE is lined on the nucleoplasmic side with a meshwork of lamin intermediate filaments constituting the nuclear lamina. Lamin depletion reduces nuclear size (Jenkins et al., 1993; Newport et al., 1990), and disease-causing mutations in lamins and lamin-associated proteins alter nuclear size and shape (Dechat et al., 2008). The NE breaks down prior to mitosis in most animal cells, and upon its reformation, the nucleus expands in a process that requires protein import (Neumann and Nurse, 2007; Newport et al., 1990), accompanied by insertion of new NPCs (D'Angelo et al., 2006). The classical nuclear import pathway is mediated by a family of importin α transport receptors that bind nuclear localization signal (NLS)-containing proteins and importin β, the protein that directs translocation through the NPC. Generation of Ran-GTP by its guanine exchange factor in the nucleus ensures unidirectional import, as only Ran in its GTP-bound state binds importin β, thereby releasing importin α and NLS cargos within the nucleus. Importin β bound to Ran-GTP is recycled to the cytoplasm, where nucleotide hydrolysis takes place, and Ran-GDP is then imported by the dedicated transport factor Ntf2, promoting another round of Ran-GTP production and cargo release (Madrid and Weis, 2006; Stewart, 2007).

One approach to studying nuclear size control is to investigate scaling, the phenomenon that nuclear size often correlates with cell size. Two related frog species exemplify scaling: *Xenopus laevis* animals, cells, and eggs are larger than *Xenopus tropicalis* (Horner and Macgregor, 1983). A significant advantage of this system is that cell-free extracts prepared from *Xenopus* eggs reconstitute assembly of subcellular structures and

organelles in vitro, including the nucleus and mitotic spindle (Maresca and Heald, 2006). Thus, it is possible to examine intrinsic mechanisms of organelle scaling in a cell-free environment. By this approach, *Xenopus* species-specific scaling by cytoplasmic factors has been demonstrated for the mitotic spindle (Brown et al., 2007). Evidence for scaling of the nucleus by cytoplasmic factors comes from experiments in fission yeast showing that nuclear size correlated with the relative amount of surrounding cytoplasm (Neumann and Nurse, 2007).

In this study, we demonstrate that nuclear size scales between *X. laevis* and *X. tropicalis* and that titratable cytoplasmic factors influence nuclear size to a greater extent than DNA content. We find that importin α and Ntf2 levels mediate interspecies nuclear scaling, at least in part, by regulating the import of lamin B3. Whereas importin α regulates the overall import rate of NLS cargos, Ntf2 modulates import based on cargo size. We further demonstrate that nuclear size scales during early *X. laevis* development and that, similar to our findings in egg extracts, changes in nuclear import and importin α levels contribute to these developmentally regulated nuclear size changes.

RESULTS

Nuclear Size and Import Scale between *X. laevis* and *X. tropicalis* In Vitro

Nuclei were assembled in *X. laevis* and *X. tropicalis* egg extracts, using *X. laevis* sperm as the chromatin source. At different time points, nuclei were fixed, visualized by immunofluorescence with an antibody against the NPC (Figure 1A), and quantified for NE surface area (Figure 1B). Nuclei assembled within 30–40 min after chromatin addition and were initially similar in size in both extracts but, over time, grew larger in *X. laevis* extract compared to *X. tropicalis*. Though nuclei in these extracts do not attain a steady-state size, *X. tropicalis* nuclei never reach the size of *X. laevis* nuclei. Extracts prepared from different batches of eggs exhibited some variability, but analysis of five extracts for each species yielded an average NE expansion rate of 70 ± 9 μm^2/min in *X. laevis* and 30 ± 9 μm^2/min in *X. tropicalis* (mean ± SD, Figure 1B). On average, NE surface area was 2.3-fold greater in *X. laevis* extract compared to *X. tropicalis*. Similar interspecies nuclear growth differences were observed in live samples by time-lapse fluorescence microscopy visualizing nuclear import of green fluorescent protein (GFP) fused to the classical SV40 NLS (Movie S1 and Figure S1A available online). To address whether continual nuclear expansion was a peculiarity of the extract system, we measured nuclear size over time in early cleavage stage *X. laevis* embryos. Nuclei expanded in vivo at a rate comparable to that of egg extracts and failed to reach a steady-state size in arrested embryos (Figure S1B), demonstrating that extracts faithfully recapitulate nuclear dynamics in the early embryo, where cell-cycle timing sets the limit for nuclear growth.

Mixing the two extracts at different ratios produced a graded effect on nuclear size (Figure 1C), suggesting that neither extract possesses dominant activating or inhibitory factors. Addition of extract fractionated by high-speed centrifugation to preassembled nuclei revealed that cytosol had a greater effect on nuclear size than membrane (data not shown). When nuclei were formed with reduced DNA content, using *X. tropicalis* sperm with 55% the DNA of *X. laevis* sperm, only an average 12% reduction in nuclear surface area was observed (Figure 1D). Taken together, these results demonstrate that, in this system, titratable cytoplasmic factors determine nuclear size to a greater extent than the amount of nuclear DNA. *X. laevis* sperm nuclei were used in all subsequent egg extract experiments, and the species denotes whether nuclei were formed in *X. laevis* or *X. tropicalis* extracts.

Of interest, we observed that GFP-NLS accumulated at a faster rate and to a greater overall extent in *X. laevis* nuclei compared to *X. tropicalis* in both live and fixed samples (Figure 1E, Figure S1C and S1D, and Movie S1). To elucidate this difference in nuclear import capacities between the two species, we first considered their nuclear pores. During early NE expansion, the total NPC number was similar in *X. laevis* and *X. tropicalis* nuclei, with a slightly higher density in *X. tropicalis* (Figure S1E and S1F). Because nuclear growth is accompanied by new NPC insertion (D'Angelo et al., 2006), the total NPC number increased more over time in *X. laevis* nuclei than in *X. tropicalis* nuclei, whereas the NPC densities remained comparable (Figures S1E and S1F). Whereas NPC number did not correlate with nuclear size during early NE expansion, there was a marked difference in their import properties. Large cargos consisting of streptavidin-conjugated quantum dots (Qdots) coated with a biotin-labeled domain of snurportin-1 that binds importin β (Lowe et al., 2010) were efficiently imported into *X. laevis* nuclei but failed to accumulate in *X. tropicalis* nuclei over time, although they localized to the NE (Figure 1F). These 40 ± 9 nm diameter particles are similar in size to a 20 megadalton macromolecule. Thus, *X. laevis* nuclei are capable of importing larger cargos than *X. tropicalis* and have a higher overall import capacity for NLS-containing proteins.

Importin α2 and Ntf2 Levels Differ between *X. laevis* and *X. tropicalis*

Given the observed nuclear import differences in the two extracts, we measured the relative amounts of nucleocytoplasmic transport proteins by western blot and immunofluorescence to determine whether concentrations of any of these proteins correlated with import. Whereas the levels of many transport factors, including Ran, RanGAP, RanBP1, and Cas, were similar in the two extracts, the concentration of the predominant importin α isoform, a member of the importin α2 subfamily, was 3-fold higher in *X. laevis* compared to *X. tropicalis* (Figure 2A and Figure S2). Levels of importin α1, importin α3, and importin β were also higher in *X. laevis* but to a lesser degree (Figure 2A and Figure S2). Furthermore, *X. laevis* nuclei stained more intensely for importin α2 and importin β than *X. tropicalis* nuclei (Figures 2B and 2C).

In contrast, Ntf2 showed the opposite trend compared to importin α, with levels almost 4-fold higher in *X. tropicalis* extract, and more intense Ntf2 nuclear staining (Figure 2). As Ntf2 is the nuclear import factor dedicated to recycling Ran-GDP from the cytoplasm to the nucleus (Smith et al., 1998), these higher Ntf2 levels likely explain why nuclear Ran was greater in *X. tropicalis* compared to *X. laevis*, even though total Ran levels were similar

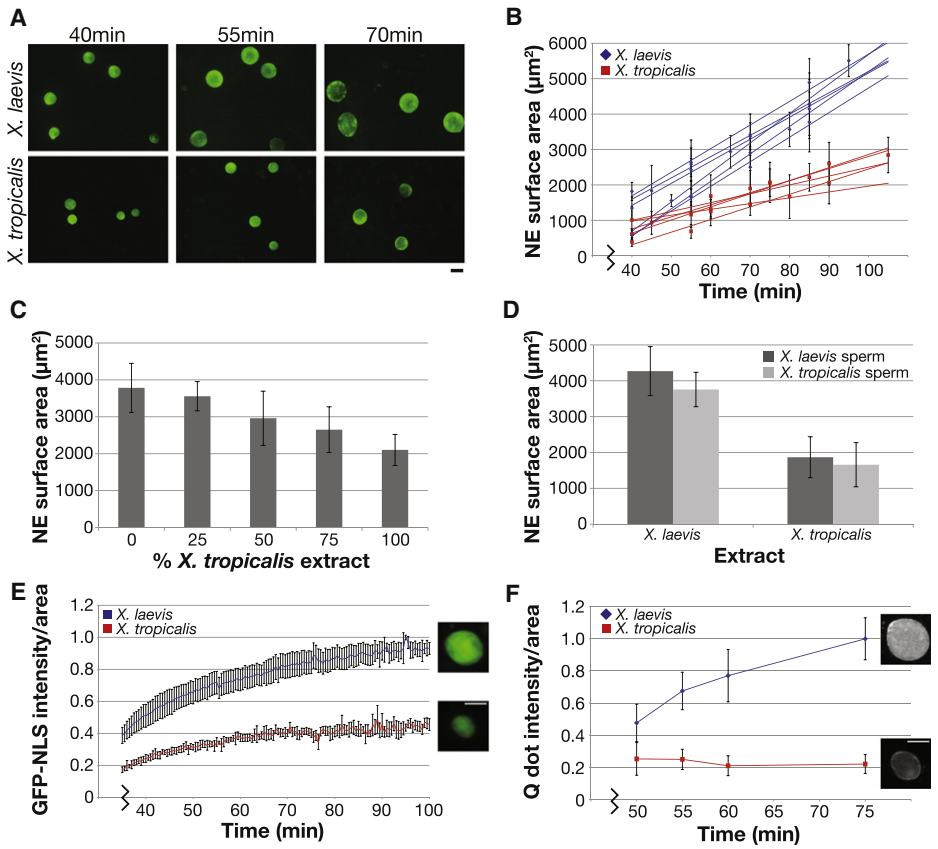

Figure 1. Nuclear Size and Import Scale between *X. laevis* and *X. tropicalis*

(A) Nuclei were assembled in *X. laevis* or *X. tropicalis* egg extract with *X. laevis* sperm and visualized by immunofluorescence using mAb414 that recognizes the NPC. Scale bar, 20 μm.

(B) NE surface area was quantified from images like those in (A) for at least 50 nuclei at each time point. Best-fit linear regression lines are displayed for six *X. laevis* and five *X. tropicalis* egg extracts, and the average difference between the two extracts was statistically significant by Student's t test ($p < 0.001$). R^2 values range from 0.96 to 0.99 for *X. laevis* and 0.94 to 0.98 for *X. tropicalis*. Error bars represent standard deviation (SD).

(C) *X. laevis* and *X. tropicalis* extracts were mixed as indicated, and nuclear size was measured at 90 min. One representative experiment of three is shown, and error bars represent SD.

(D) Nuclei were assembled using the indicated source of extract and sperm, and nuclear size was measured at 90 min. One representative experiment of three is shown, and error bars represent SD.

(E) GFP-NLS was added to nuclei at 30 min, and images were acquired live at 30 s intervals with the same exposure time. Nuclear GFP-NLS fluorescence intensity per unit area was measured at each time point, averaged for five nuclei from each extract, and normalized to 1.0 (arbitrary units). Error bars represent SD. Representative images are at 70 min. Scale bar, 20 μm.

(F) IBB-coated Qdots were added to nuclei at 30 min, and images were acquired live at the indicated time points for at least 30 nuclei with the same exposure time. Nuclear Qdot fluorescence intensity per unit area was calculated, averaged, and normalized to 1.0 (arbitrary units). Error bars represent SD. One representative experiment of three is shown. Representative images are at 75 min. Scale bar, 20 μm.

See also Figure S1 and Movie S1.

(Figure 2). The marked differences in importin α2 and Ntf2 concentrations led us to investigate their relevance to nuclear scaling between the two species.

Importin α2 Increases Nuclear Size and Import

First, we altered importin α levels. Endogenous importin α must be phosphorylated to diffuse freely in *Xenopus* cytoplasm while the unphosphorylated form binds large membrane stores present in egg extracts (Hachet et al., 2004), possibly rendering it unable to engage in nucleocytoplasmic transport. We therefore tested the effects of a phosphomimetic importin α-E containing six glutamate point mutations (Hachet et al., 2004), as well as in vitro phosphorylated importin α (Hachet et al., 2004). When added to nuclei assembled in *X. tropicalis* egg extract, both of these proteins increased NE surface area, whereas unphosphorylated importin α had little effect (Figure S3A). The maximal change in nuclear size occurred in the range of 0.8–1 μM added importin α-E, increasing NE surface area 1.5- to 1.7-fold (Figure 3A). Importin α-E likely affects nuclear size by modulating import because its addition increased nuclear accumulation of GFP-NLS and addition of import-defective importin α-E lacking the N-terminal importin β-binding (IBB) domain failed to increase nuclear size (Figure 3B and Figure S3A).

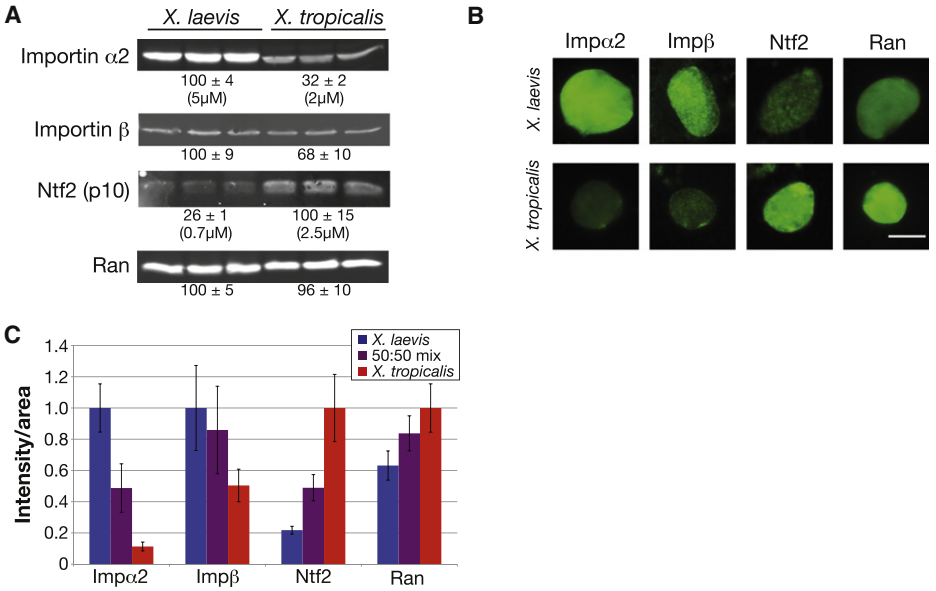

Figure 2. Importin α2 and Ntf2 Levels Differ in *X. laevis* and *X. tropicalis*

(A) 25 μg of protein from three different *X. laevis* and *X. tropicalis* egg extracts was separated by SDS-PAGE, transferred to nitrocellulose, and probed with antibodies against the indicated proteins. Values below each set of three lanes represent relative protein amounts (mean ± SD, n = 3) quantified by infrared fluorescence. Absolute concentrations were determined by comparing band intensities to known concentrations of recombinant importin α2 or Ntf2 on the same blot. Two different antibodies against importin α2 and Ntf2 showed similar differences between the two species.

(B) Nuclei at 80 min were processed for immunofluorescence using the same antibodies as in (A), and representative images are shown. For a given antibody, images were acquired with the same exposure time and scaled identically. Scale bar, 20 μm.

(C) Quantification of nuclei displayed in (B). Nuclear fluorescence intensity per unit area was calculated for at least 50 nuclei per condition, averaged, and normalized to 1.0 (arbitrary units). Error bars represent SD. Two different antibodies against importin α2 and Ntf2 showed similar differences between the two species. See also Figure S2.

In complementary experiments, importin α2 was partially immunodepleted from *X. laevis* extracts. Depending on the extract, 0.5–1 μM importin α2 was depleted, and no other proteins were stoichiometrically codepleted (data not shown). Compared to mock-depleted extracts, lowering the importin α concentration reduced nuclear size and GFP-NLS import, and both effects could be rescued by addition of importin α-E but only if it was import competent with an intact IBB domain (Figure 3C). Addition of excess importin α-E to *X. tropicalis* nuclei (Figure 3A) or *X. laevis* nuclei (data not shown) slightly reduced nuclear size while minimally affecting bulk import.

To address the specificity of the importin α effect and to determine whether other import factors contribute to nuclear sizing, we added importin α-E, importin β, and Ran alone and in combination to nuclei assembled in *X. tropicalis* extract. At 0.8 μM, importin β negatively affected nuclear size, Ran had no effect, and no combination with importin α-E increased nuclear size to a greater extent than importin α-E alone (Figure S3B). At 4 μM, all three proteins individually reduced nuclear size, and no combination increased size (Figure S3B). We also investigated a different Ran-regulated nucleocytoplasmic shuttling pathway that utilizes the transport receptor transportin. Addition of recombinant transportin to *X. tropicalis* nuclei negatively affected nuclear size at all concentrations tested, likely by interfering with other Ran-mediated transport (Figure S3C). Furthermore, transportin levels were indistinguishable between *X. laevis* and *X. tropicalis* (Figure S2), as was nuclear import of YFP-M9-CFP, a transportin cargo (Figure S3D). We conclude that nuclear scaling acts predominantly through the NLS-mediated import pathway, in particular through importin α.

Ntf2 Decreases Nuclear Size and Import of Large Cargos

Although importin α contributes to nuclear scaling, its effect was insufficient to explain the average 2.3-fold size difference between *X. laevis* and *X. tropicalis* nuclei. Because Ntf2 was the only other import factor we identified that differed significantly between the two extracts (Figure 2), being more abundant in *X. tropicalis*, recombinant Ntf2 was titrated into *X. laevis* extract. Increasing the Ntf2 concentration increased nuclear Ran, consistent with functional Ntf2 directing Ran import, and nuclear size was concomitantly reduced (Figure 3D). When 1.6 μM Ntf2 was added to *X. laevis* extract to approximate the total Ntf2 concentration in *X. tropicalis*, nuclear Ran staining increased to nearly the *X. tropicalis* level, but NE surface area was not fully reduced to that of *X. tropicalis*. Intriguingly, GFP-NLS import did not correlate with nuclear size. In fact, addition of Ntf2 slightly increased nuclear GFP-NLS levels, perhaps due to the higher nuclear Ran concentration (Figure 3D). This result suggested that Ntf2 was not affecting nuclear size by altering the global NLS import rate. Instead, increasing the Ntf2 concentration in *X. laevis* reduced the amount and rate of Qdot import (Figures 3D and 3E). Because Ntf2 binds proteins of the NPC (Clarkson et al., 1996), higher Ntf2 levels may occlude the pore, potentially impeding import of larger particles like Qdots,

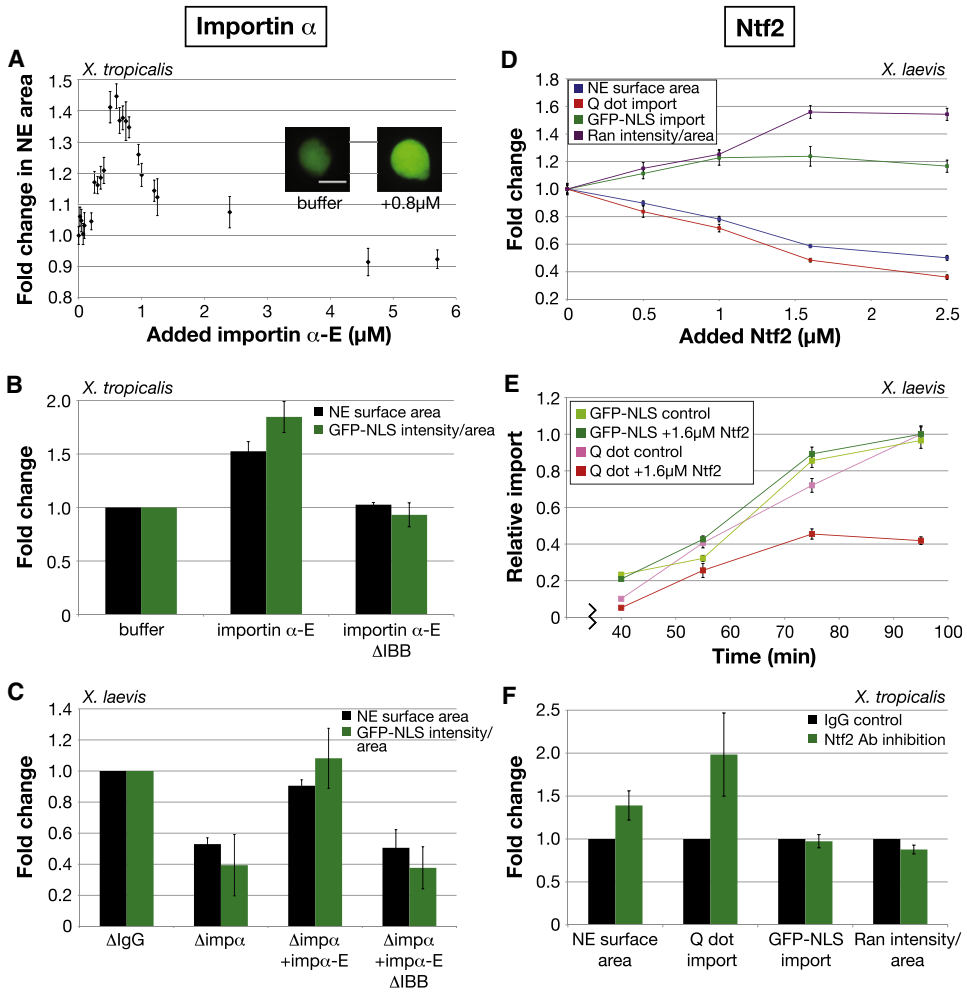

Figure 3. Importin α2 and Ntf2 Regulate Nuclear Size and Import

(A) Nuclei were assembled in *X. tropicalis* extract, and at 40 min, importin α-E was added at the indicated concentrations in addition to GFP-NLS. At 80 min, images for at least 50 nuclei per condition were acquired with the same exposure time, and NE surface area was quantified, averaged, and normalized to the buffer control. Error bars represent standard error (SE). Scale bar, 20 μm.

(B) Experiments were performed as in (A) with a fixed concentration (0.8 μM) of added importin α-E or a mutant version lacking the importin β-binding domain (ΔIBB). Average fold change from the buffer control and SD are shown (n = 4 extracts). The ΔIBB mutant did not have a strong dominant-negative effect on import because it was added at a concentration below the endogenous importin α level.

(C) Nuclei were assembled in *X. laevis* extract mock and partially immunodepleted of importin α2 (0.5–1 μM depleted). Kinetics of nuclear assembly were similar in the two extracts. At 40 min, indicated proteins were added at 1 μM as well as GFP-NLS. At 80 min, images for at least 50 nuclei per condition were acquired with the same exposure time, and NE surface area and nuclear GFP-NLS fluorescence intensity were quantified. Average fold change from the mock depletion and SD are shown (n = 4 extracts).

(D) Recombinant Ntf2 was titrated into *X. laevis* extract prior to nuclear assembly. Initial kinetics of nuclear assembly were not altered by supplemental Ntf2. GFP-NLS or IBB-coated Qdots were added at 30 min. At 80 min, nuclei were processed for immunofluorescence with an antibody against Ran, and images for at least 50 nuclei per condition were acquired with the same exposure time. NE surface area was quantified from Ran-stained nuclei, averaged, and normalized to the buffer control. Nuclear fluorescence intensities for Qdots, GFP-NLS, and Ran were similarly processed. Error bars represent SE. One representative experiment of three is shown. For each parameter, the difference between 0 and 1.6 μM added Ntf2 was statistically significant by Student's t test ($p < 0.005$).

(E) Experiments similar to (D) were performed with a fixed Ntf2 concentration (1.6 μM) and over time. Nuclear Qdot or GFP-NLS fluorescence intensities for at least 50 nuclei per time point were averaged and normalized to 1.0 (arbitrary units). Error bars represent SE. At 95 min, the difference in Q dot import between 0 and 1.6 μM added Ntf2 was statistically significant by Student's t test ($p < 0.001$).

(F) Nuclei were assembled in *X. tropicalis* extract supplemented with anti-Ntf2 or IgG antibodies (0.1 mg/ml). At 30 min, nuclear assembly was similar in the two conditions, and Qdots or GFP-NLS was added. At 80 min, immunofluorescence for Ran was performed, and nuclear parameters were quantified as in (D). Average fold change from the IgG control and SD are shown (n = 6 extracts).

See also Figure S3.

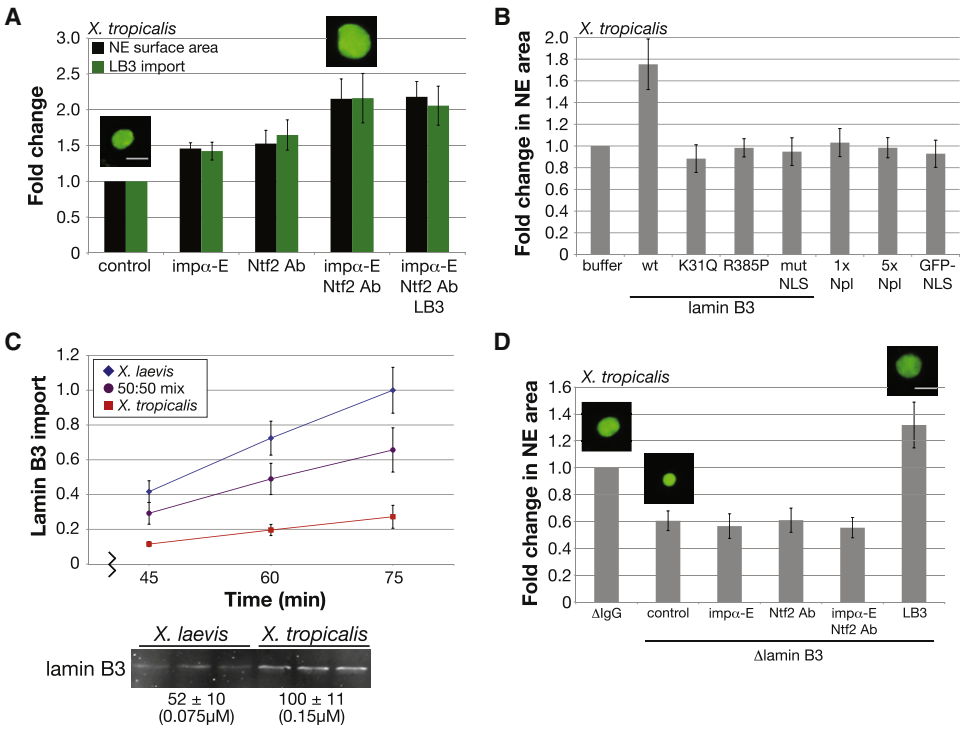

Figure 4. Importin α2 and Ntf2 Are Sufficient to Account for Interspecies Nuclear Scaling by Regulating LB3 Import

(A) *X. tropicalis* nuclei were assembled in the presence of anti-Ntf2 or IgG control antibodies (0.1 mg/ml) and 0.14 μM GFP-LB3 as indicated, and at 40 min, 0.8 μM importin α-E was added to some reactions. LB3 was visualized in nuclei by immunofluorescence at 80 min, and images for at least 50 nuclei per condition were acquired with the same exposure time. NE surface area and LB3 fluorescence were quantified. Average fold change from the buffer control and SD are shown (n = 5 extracts). Scale bar, 20 μm.

(B) Wild-type and mutant GFP-LB3 proteins, 1 × Npl (nucleoplasmin), and GFP-NLS were added at 0.14 μM to *X. tropicalis* extract. For 5 × Npl, 0.7 μM Npl was added. Nuclei were visualized at 75 min by immunofluorescence using an antibody against Ran. NE surface area was calculated for at least 50 nuclei. Average fold change from the buffer control and SD are shown (n = 3 extracts). The K31Q mutant had a dominant-negative effect on the structure of the lamina, as nuclei were smaller and appeared crumpled, whereas the R385P mutant did not efficiently assemble into the lamina.

(C) Nuclei were visualized by immunofluorescence with an antibody against *Xenopus* LB3. Images for at least 50 nuclei at each time point were acquired with the same exposure time. Fluorescence intensity was quantified, averaged, and normalized to 1.0 (arbitrary units). Error bars represent SD. One representative experiment of three is shown. The Western blot was performed as in Figure 2A using an antibody against *Xenopus* LB3.

(D) Nuclei were assembled in *X. tropicalis* extract mock- and immunodepleted of LB3 (0.1 μM depleted). Ntf2 antibodies, importin α-E, and GFP-LB3 were added to LB3-depleted extract in the same manner as in (A) with the exception that GFP-LB3 was added at 0.2 μM. At 80 min, nuclei were stained for Ran by immunofluorescence, images for at least 50 nuclei per condition were acquired, and NE surface area was quantified. Average fold change from the mock depletion and SD are shown (n = 4 extracts). Scale bar, 20 μm.

See also Figure S4 and Table S1.

but not small cargos like GFP-NLS. Consistent with this model, reducing the effective Ntf2 concentration in *X. tropicalis* by antibody inhibition (Figure 3F) or Ntf2 depletion (Figure S3E) conferred on these nuclei the ability to import Qdots without significantly altering GFP-NLS import. Concomitantly, NE surface area increased 1.4- to 1.5-fold, and nuclear Ran staining decreased on average 11% (Figure 3F and Figure S3E). Taken together, these data are consistent with Ntf2 regulating nuclear size by modulating the import rates of large cargos that presumably contribute to nuclear sizing.

Importin α2 and Ntf2 Scale Nuclear Size through Lamin B3 Import

Because both addition of importin α and inhibition of Ntf2 in *X. tropicalis* increased nuclear size, we tested whether combining these manipulations was sufficient to convert *X. tropicalis* nuclei to the size of *X. laevis* nuclei. Averaged over five experiments, *X. tropicalis* NE surface area increased 2.2-fold with supplemental importin α-E and Ntf2 inhibition (Figure 4A), nearly equivalent to the average 2.3-fold interspecies nuclear size difference (Figure 1B).

Importin α and Ntf2 could control nuclear size by regulating either bulk import of NLS cargos or import of specific structural components of the nucleus. To differentiate between these possibilities, we supplemented *X. tropicalis* extract with different NLS cargos to specifically increase their import and assessed the effect on nuclear size. Addition of nucleoplasmin (Npl) or GFP-NLS, both importin α cargos, did not significantly alter nuclear size over a wide range of concentrations (Figure 4B, Figure S4A, and data not shown). In contrast, recombinant lamin B3 (LB3) titrated into *X. tropicalis* extract increased NE surface area 1.7-fold when added at an optimal concentration of 0.14 μM (Figure 4B and Figure S4A). LB3 is the major *Xenopus* egg lamin

that is required for NE growth (Jenkins et al., 1993; Newport et al., 1990) and contains a classical NLS (Loewinger and McKeon, 1988). At higher concentrations of LB3, nuclear size was reduced and LB3 puncta were visible, likely representing the formation of aggregates unable to assemble into a functional lamina (Figure S4A). Addition of two LB3 point mutants previously shown to be defective for lamina assembly (Heald and McKeon, 1990), or LB3 with a mutated NLS, failed to increase nuclear size (Figure 4B). These data indicate that the concentration of the specific cargo LB3 can determine nuclear size, dependent on its import and functional assembly.

Because LB3 concentration can affect nuclear size, we compared LB3 import and levels in the two *Xenopus* extracts. Although the rate of nuclear LB3 accumulation in *X. tropicalis* extract was 35% the rate in *X. laevis*, the LB3 concentration was ~2-fold higher in *X. tropicalis* (Figure 4C), consistent with the *X. laevis* egg containing 2.1-fold more total LB3 in a 4.3-fold larger volume (Table S1). Nuclear size differences in these two extracts therefore correlate not with lamin concentration but, rather, with the rate of lamin import as regulated by importin α and Ntf2. Consistent with this interpretation, upon addition of importin α and inhibition of Ntf2 in *X. tropicalis* that led to increased LB3 import, supplemental LB3 did not further increase nuclear size (Figure 4A and Figures S4B and S4C). Conversely, Ntf2 reduced import of LB3 in a concentration-dependent manner in *X. laevis* (Figure S4D). Furthermore, addition of importin α and/or Ntf2 antibodies to LB3-depleted *X. tropicalis* extracts had little effect on nuclear size (Figure 4D), even though these nuclei were still import competent for GFP-NLS (data not shown). Taken together, these data argue that differences in importin α and Ntf2 concentrations can account for nuclear scaling between *X. laevis* and *X. tropicalis* and that they control nuclear size by regulating import of LB3 and possibly other NLS cargos that require an intact lamina to function.

Nuclear Scaling during *Xenopus* Development Is Also Regulated by Importin α

To investigate whether mechanisms of interspecies nuclear scaling also operate during development, we turned to *X. laevis* embryos. Upon fertilization, the 1 mm diameter egg undergoes 12 rapid, synchronous cell divisions (each ~30 min) with no overall growth, generating about four-thousand 50 μm cells at the midblastula transition (MBT) or stage 8 (Nieuwkoop and Faber, 1967). After the MBT, zygotic transcription initiates, cells become motile, and cell divisions slow and lose synchrony. As the embryo proceeds through gastrulation, further reductions in cell size occur, reaching 12 μm in the tadpole (Montorzi et al., 2000). *Xenopus* embryogenesis therefore offers a robust model for developmental scaling.

Nuclear size was quantified in *X. laevis* embryos by immunofluorescence (Figure 5A). Because nuclei continually expand in early embryos (Figure S1B), we compared different stage embryos arrested for 60 min. Though nuclear sizes were similar during the first few cell divisions after fertilization, NE surface area became progressively smaller after stage 5 (16 cell) and through stage 10 (gastrulation), reaching a relatively constant size in stage 12 and later embryos. Measurements made in situ were comparable (Figure S5A). A similar trend in nuclear size changes was observed in *X. tropicalis* embryos except NE surface area was on average 51% less than *X. laevis* at equivalent developmental stages (Figure S5B). Halving the DNA content in *X. laevis* embryonic nuclei only reduced NE surface area by 10%, demonstrating that, like egg cytoplasm, embryo cytoplasm determines nuclear size to a greater extent than ploidy (Figure S5C).

To investigate whether nucleocytoplasmic transport also regulates nuclear scaling during early *X. laevis* development, we examined the levels of transport factors. Strikingly, total importin α2 levels dropped 47% by stage 8 (MBT) relative to earlier stages and a further 30% by stage 12 (Figure 5B). In contrast, importin α1, importin α3, Ran, and Ntf2 concentrations remained relatively constant (Figure 5B and Figure S5D). At stage 8, concomitant reductions in GFP-NLS import capacity and nuclear importin α2 and Ntf2 staining occurred, whereas, at stage 12, import was reduced further but with no significant change in nuclear importin α2 and Ntf2 (Figures 5C and 5D).

To determine whether importin α directly modulates nuclear size during development, fertilized one-cell *X. laevis* embryos were injected with mRNA encoding importin α-E and were allowed to develop to later stages. Exogeneous expression of importin α-E to 0.6 μM ± 0.2 μM (mean ± SD, n = 5) significantly increased nuclear size in stage 7 and stage 8 embryos to the range observed in early stage embryos but had a lesser effect at stage 9 (Figure 5E). Increasing nuclear size in embryos did not affect their gross morphology or viability. Addition of importin α-E to embryo extracts similarly increased nuclear size (Figure S5E) and also increased GFP-NLS import (data not shown), whereas Ntf2 addition had little effect (data not shown). Of interest, we observed that nuclei in stage 7 and stage 8 embryos reached a steady-state size (Figure 5F), unlike earlier in development (Figure S1B). Overexpression of importin α-E in stage 7 embryos led to continuous nuclear expansion similar to that observed in early stages, whereas nuclei in stage 8 embryos grew larger but attained a new equilibrium size, suggesting that other factors became limiting at the MBT (Figure 5F). Taken together, these data demonstrate that importin α is one factor that mediates nuclear scaling during *X. laevis* embryogenesis, affecting both the rate of nuclear expansion in early embryos and the steady-state nuclear size in later embryos.

DISCUSSION

We investigated how nuclear size is regulated in two related but different sized frog species as well as during early frog development, two physiological examples of nuclear scaling. Using *Xenopus* egg extracts to examine intrinsic mechanisms of nuclear scaling in the absence of the cell showed that titratable cytoplasmic factors regulate nuclear size to a greater extent than DNA content and that differences in the concentrations of importin α and Ntf2 are sufficient to explain most of the observed interspecies nuclear scaling by altering nuclear import. Importin α, but not Ntf2, also plays a role in nuclear scaling during embryogenesis in *X. laevis*. Whereas nucleocytoplasmic transport was known to be required for NE growth (D'Angelo et al.,

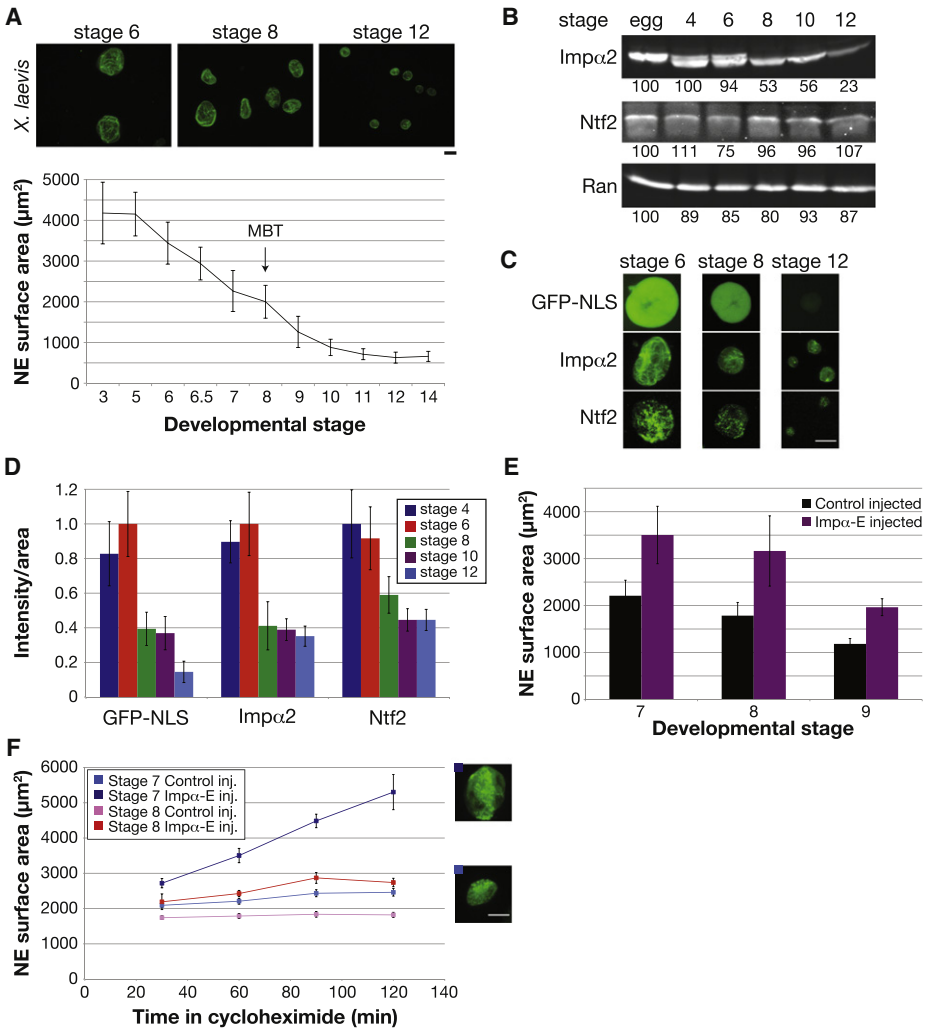

Figure 5. Importin α2 Regulates *X. laevis* Developmental Nuclear Scaling

(A) Different stage *X. laevis* embryos were arrested with cycloheximide for 60 min. Nuclei were isolated from embryo extracts and visualized by immunofluorescence using mAb414. Scale bar, 20 μm. For the graph, NE surface area was quantified for at least 50 nuclei from each stage. Error bars represent SD.

(B) 25 μg of protein from different stage embryo extracts was analyzed by western blot, as in Figure 2A.

(C) To assess nuclear import, GFP-NLS (1 μM) was added to embryo extracts, and images of unfixed nuclei were acquired 30 min later with the same exposure time. Immunofluorescence was performed on fixed embryonic nuclei, and images were acquired with the same exposure time. Scale bar, 20 μm.

(D) Quantification of (C). Nuclear fluorescence intensity per unit area was calculated for at least 50 nuclei per stage, averaged, and normalized to 1.0 (arbitrary units). Error bars represent SD.

(E) Single-cell fertilized *X. laevis* embryos were injected with 1 ng importin α-E mRNA or water as control. Nuclei were isolated and quantified as in (A), except that an antibody against *Xenopus* LB3 was used for immunofluorescence. One representative experiment of two is shown for each stage, and error bars represent SD.

(F) Experiments similar to (E) were performed except that embryos were arrested for different lengths of time in cycloheximide. Error bars represent SE. Representative stage 7 nuclei at 120 min are shown for control (bottom) and importin α-E (top) injected embryos. Scale bar, 20 μm.

See also Figure S5.

2006; Neumann and Nurse, 2007; Newport et al., 1990), our data show that titrating nuclear import concomitantly scales nuclear size and that this mechanism can account for how the size of the nucleus is controlled in two frog species and during development.

Importin α mediates nuclear scaling by regulating overall import of NLS cargos, consistent with computer modeling and cell culture experiments showing that importin α concentration positively correlates with the rate and steady-state level of nuclear import (Görlich et al., 2003; Riddick and Macara, 2005, 2007; Smith et al., 2002). However, our results indicate a more complex relationship between nuclear import factors and nuclear size. For example, we observe that increasing importin α concentration more than 3-fold over normal levels reduces nuclear size (Figure 3A and Figure S3B), probably because elevated lamin B3 import that occurs under these conditions (data not shown) is detrimental to nuclear assembly (Figure S4A). Ntf2 has also been implicated as a positive

regulator of both Ran and bulk import (Riddick and Macara, 2005, 2007). Though the Ntf2-Ran relationship holds true in our experiments, we find that increased Ntf2 slows import of large cargos such as Qdots, but not smaller proteins like GFP-NLS. Because it associates with the NPC, Ntf2 could influence import rates based on cargo size (Clarkson et al., 1996). In fact, studies of *X. laevis* oogenesis revealed that late-stage oocytes acquire the ability to import large nucleoplasmin-coated gold particles concomitantly with a reduction in Ntf2 levels (Feldherr et al., 1998). Furthermore, addition of Ntf2 to those oocytes reduced import of gold particles, similar to our observation that increasing the Ntf2 concentration in *X. laevis* reduced Qdot import (Figure 3D). It is worth noting that supplementing *X. laevis* extract with Ntf2 up to the *X. tropicalis* level slowed but did not block Qdot import, suggesting that other interspecies NPC differences may affect cargo size-dependent import.

Nuclear size appears to be determined by import of specific NLS cargos, not by mass action transport. LB3 was a good candidate because its import is importin α-mediated, it is required for NE expansion (Jenkins et al., 1993; Newport et al., 1990), and its overexpression induces proliferation of nuclear membrane (Goldberg et al., 2008; Prüfert et al., 2004). Addition of LB3, but not Npl or GFP-NLS, to *X. tropicalis* egg extract increased nuclear size, but not to the size of *X. laevis*, suggesting that additional NLS proteins are involved. Potential nuclear sizing cargos include inner nuclear membrane proteins that interact with the lamina, like the lamin B receptor and LAPs, as well as SUN and KASH family proteins that span the NE and mediate interactions between the nucleus and cytoskeleton. Consistent with this idea, NPC manipulations that increase translocation of integral membrane proteins to the inner NE correlate with increased nuclear size (Theerthagiri et al., 2010). The fact that Qdot import positively correlates with nuclear size indicates that cargos important for scaling are relatively large. Although lamin monomers are only 70 kD, they minimally form tetramers made up of two dimers, each composed of 50 nm elongated coiled coils (Aebi et al., 1986; Heitlinger et al., 1991). Because particles as large as 20 megadaltons can transit the *X. laevis* NPC, LB3 may be imported as large oligomers.

We discovered some striking similarities between interspecies nuclear size regulation and nuclear scaling during *Xenopus* embryogenesis. Reductions in nuclear size during development were accompanied by diminishing import capacity for NLS cargos, and scaling of nuclear size at the MBT correlated with a drop in total and nuclear importin α levels. Increasing the concentration of importin α in embryos increased nuclear size without noticeably affecting development, suggesting that nuclear size per se does not regulate early developmental transitions. Thus, conserved importin α-mediated transport mechanisms regulate nuclear size both during development and between frog species, but distinct and yet uncharacterized mechanisms also contribute to nuclear scaling in *Xenopus* embryogenesis.

Our data suggest two nuclear sizing regimes determined by either reaction rates or abundance of NE components. The egg is stockpiled in order to form ~4000 MBT nuclei, and therefore these components are not limiting in egg extracts and early embryos. In this regime, nuclear size is determined by rates of NE expansion and nuclear import in conjunction with cell-cycle timing. In contrast, MBT nuclei reach a steady-state size when import and NE components like lamins are no longer in excess. Consistent with this idea, increasing importin α expression in MBT embryos caused nuclei to reach a new steady-state size (Figure 5F) at which lamins became limiting because coexpressing importin α and LB3 further augmented nuclear size (data not shown). Of interest, the amount of LB3 loaded into the eggs of each species correlates well with the total NE surface area at the MBT, with *X. laevis* containing 2.1-fold more total LB3 than *X. tropicalis* at the onset of development and 2-fold more NE at the MBT when transcription starts (Table S1). Because the ratio of NE surface area to embryo volume at this transition is 2.1-fold higher in the smaller *X. tropicalis* species (Table S1), the starting LB3 concentration in the egg is also about 2-fold higher (Figure 4C). Thus *Xenopus* eggs are loaded with the proper amount of LB3, and presumably other nuclear envelop components, so that they are not limiting during the rapid divisions of early development.

Our results are consistent with multiple mutually nonexclusive models of organelle size control. Considering a static model, importin α and Ntf2 levels limit nuclear import of LB3, thereby constraining the rate at which nuclei expand. However, dynamic processes must balance import-mediated growth. Nuclear size is a regulated cellular parameter that depends on tissue type, developmental state as demonstrated during *Xenopus* embryogenesis, and species as shown comparing *X. laevis* and *X. tropicalis*, in which nuclear size differences have evolved by fine-tuning the expression of nuclear import factors. A fundamental question is why nuclear size is regulated. Changes in the dimensions and morphology of the nucleus are associated with pathologies, including cancer (Webster et al., 2009; Zink et al., 2004), but dissecting the cause and effect relationship between nuclear size and disease state is difficult. Understanding the role that nuclear import plays in scaling nuclear size and identifying relevant factors and their mechanisms of action provide an avenue to directly manipulate nuclear size in the context of normal and diseased cells in order to examine the functional consequences.

EXPERIMENTAL PROCEDURES

Xenopus Egg Extracts and Nuclear Assembly

X. laevis (Maresca and Heald, 2006) and *X. tropicalis* (Brown et al., 2007) metaphase-arrested egg extracts and *Xenopus* sperm (Murray, 1991) were made as previously described. The standard nuclear assembly reaction was 25 μl fresh extract, 100 μg/ml cycloheximide, 1000 *Xenopus* sperm per μl, and 0.5 mM $CaCl_2$. *X. laevis* sperm was used in all experiments except Figure 1D, in which *X. tropicalis* sperm was used, as indicated. Reactions were incubated at 19°C–22°C and import-competent nuclei generally formed within 30–40 min.

To monitor nuclear import, GFP-NLS (1 μM), YFP-M9-CFP (1 μM), or IBB-Qdots (10 nM) were added to nuclei. IBB-Qdots were prepared by mixing 20 μM biotin-labeled IBB-CFP (a gift from Alan Lowe and Jan Liphardt) with 1 μM Qdot 605 streptavidin conjugate (Invitrogen) at a 1:1 ratio and incubating on ice 15 min. We also examined import of three smaller IBB-Qdots using Qdots 525, 565, and 585 streptavidin conjugates (Invitrogen), finding that all three were imported into *X. laevis* and *X. tropicalis* nuclei (data not shown).

Immunodepletions and recombinant proteins are detailed in the Extended Experimental Procedures. Proteins and antibodies were dialyzed into XB

(100 mM KCl, 1 mM $MgCl_2$, 0.1 mM $CaCl_2$, 50 mM sucrose, and 10 mM HEPES [pH 7.7]) and added to extracts prior to nuclear assembly, except for importin α, which was dialyzed into 300 mM KCl, 10 mM $MgCl_2$, and 10 mM HEPES (pH7.8) and added to preformed nuclei. Total volume of addition was less than 10% the reaction volume, and buffer and IgG controls were performed. Reactions were allowed to proceed to 75–90 min, as nuclear size at these time points was similar to the size of nuclei in early stage embryos, thus providing a physiologically relevant situation for comparing nuclear size changes.

Xenopus Embryos and Extracts

Xenopus embryos were obtained as previously described (Grammer et al., 2005; Sive et al., 2000), and details on how they were generated and injected are in the Extended Experimental Procedures. Embryos were arrested in late interphase with 150 μg/ml cycloheximide for 60 min unless indicated otherwise (Lemaitre et al., 1998), washed several times in ELB (250 mM sucrose, 50 mM KCl, 2.5 mM $MgCl_2$, and 10 mM HEPES [pH 7.8]) containing LPC (10 μg/ml each leupeptin, pepstatin, chymostatin), cytochalasin D (100 μg/ml), and cycloheximide (100 μg/ml), packed in a tabletop centrifuge at 200 g for 1 min, crushed with a pestle, and centrifuged at 10,000 × g for 10 min at 16°C. The cytoplasmic extract containing endogenous embryonic nuclei was supplemented with LPC, cytochalasin D (20 μg/ml), cycloheximide (100 μg/ml), and energy mix (3 mM creatine phosphate, 0.4 mM adenosine triphosphate, 40 μM EGTA, and 0.4 mM $MgCl_2$).

Immunofluorescence and Microscopy

Nuclei in egg extracts or from embryos were mixed with 20 volumes fix buffer (ELB, 15% glycerol, 2.6% paraformaldehyde) for 15 min at room temperature, layered over 5 ml cushion buffer (XB, 200 mM sucrose, 25% glycerol), and spun onto 12 mm circular coverslips at 1000 × g for 15 min at 16°C. Nuclei were postfixed in cold methanol for 5 min and rehydrated in PBS-NP40. Coverslips were blocked with PBS-3% BSA overnight at 4°C, incubated at room temperature for 1 hr each with primary and secondary antibody diluted in PBS-BSA followed by 5 μg/ml Hoechst, mounted in Vectashield (Vector Laboratories), and sealed with nail polish. Antibodies are described in the Extended Experimental Procedures.

Images were acquired with an Olympus BX51 fluorescence microscope, 40× objective, and Hamamatsu Orca II cooled CCD camera. Nuclear cross-sectional areas were measured from thresholded images in MetaMorph (Molecular Devices) and multiplied by 4 to estimate total NE surface area. To validate this method for quantifying nuclear size, imaging was performed using a Marianas Spinning Disk Confocal microscope (Intelligent Imaging Innovations). For a given nucleus, 100 confocal sections were acquired, and nuclear circumference for each slice was measured in ImageJ (NIH). NE surface area was calculated as the sum of these circumferences multiplied by the slice thickness (0.2 μm), and these values agreed within 2% of estimates from the cross-sectional area (data not shown). We therefore used the cross-sectional area method to estimate NE surface area because it facilitated the acquisition of data from large numbers of nuclei. For fluorescence intensity measurements, images were acquired with the same exposure time, and a region of representative background fluorescence was used for background correction. Total integrated intensity and nuclear area were quantified from thresholded images (Metamorph) and used to calculate intensity per unit area. Statistical methods are described in the figure legends.

Western Blots

Egg extract protein concentrations were measured by Bradford assay (Biorad). The average total protein concentration was 56 ± 3 mg/ml in *X. laevis* and 52 ± 4 mg/ml in *X. tropicalis* (mean ± SD, n = 6). 25 μg protein from three different *X. laevis* and *X. tropicalis* extracts was separated by SDS-PAGE and semi-dry transferred to nitrocellulose (Biorad). Blots were blocked with PBS-5% milk, probed with primary and secondary antibodies (see Extended Experimental Procedures) diluted in PBST-5% milk, and scanned on an Odyssey Infrared Imaging System (LI-COR Biosciences). Band intensities were quantified using the Odyssey software. Western blots on different stage embryo extracts were similarly performed.

SUPPLEMENTAL INFORMATION

Supplemental Information includes Extended Experimental Procedures, five figures, one table, and one movie and can be found with this article online at doi:10.1016/j.cell.2010.09.012.

ACKNOWLEDGMENTS

We thank Steve Bird, Mary Dasso, Dirk Görlich, David Halpin, Richard Harland, Petr Kalab, Jan Liphardt, Alan Lowe, Andreas Merdes, Jon Soderholm, and Karsten Weis for reagents. We acknowledge Steve Bird and Saori Haigo for conducting the initial nuclear scaling experiments in egg extracts; Saori Haigo, Esther Kieserman, and Richard Harland's laboratory for help with *Xenopus* embryos; and Abby Dernburg for use of the Marianas SDC microscope. We thank members of the Heald lab for helpful advice; Rose Loughlin, Jeff Tang, Karsten Weis, and David Weisblat for constructive comments on the manuscript; and Favian Hernandez for artwork. R.H. is supported by the NIH Director's Pioneer Award (DP1 OD000818) and The Miller Institute for Basic Research in Science. D.L.L. acknowledges support from an American Cancer Society postdoctoral fellowship (PF-09-041-01-DDC).

Received: March 24, 2010
Revised: July 6, 2010
Accepted: September 7, 2010
Published: October 14, 2010

REFERENCES

Aebi, U., Cohn, J., Buhle, L., and Gerace, L. (1986). The nuclear lamina is a meshwork of intermediate-type filaments. Nature *323*, 560–564.

Brown, K.S., Blower, M.D., Maresca, T.J., Grammer, T.C., Harland, R.M., and Heald, R. (2007). *Xenopus tropicalis* egg extracts provide insight into scaling of the mitotic spindle. J. Cell Biol. *176*, 765–770.

Cavalier-Smith, T. (2005). Economy, speed and size matter: evolutionary forces driving nuclear genome miniaturization and expansion. Ann. Bot. *95*, 147–175.

Clarkson, W.D., Kent, H.M., and Stewart, M. (1996). Separate binding sites on nuclear transport factor 2 (NTF2) for GDP-Ran and the phenylalanine-rich repeat regions of nucleoporins p62 and Nsp1p. J. Mol. Biol. *263*, 517–524.

D'Angelo, M.A., Anderson, D.J., Richard, E., and Hetzer, M.W. (2006). Nuclear pores form de novo from both sides of the nuclear envelope. Science *312*, 440–443.

Dechat, T., Pfleghaar, K., Sengupta, K., Shimi, T., Shumaker, D.K., Solimando, L., and Goldman, R.D. (2008). Nuclear lamins: major factors in the structural organization and function of the nucleus and chromatin. Genes Dev. *22*, 832–853.

Fankhauser, G. (1939). Polyploidy in the salamander, *Eurycea bislineata*. J. Hered. *30*, 379–388.

Feldherr, C., Akin, D., and Moore, M.S. (1998). The nuclear import factor p10 regulates the functional size of the nuclear pore complex during oogenesis. J. Cell Sci. *111*, 1889–1896.

Goldberg, M.W., Huttenlauch, I., Hutchison, C.J., and Stick, R. (2008). Filaments made from A- and B-type lamins differ in structure and organization. J. Cell Sci. *121*, 215–225.

Görlich, D., Seewald, M.J., and Ribbeck, K. (2003). Characterization of Ran-driven cargo transport and the RanGTPase system by kinetic measurements and computer simulation. EMBO J. *22*, 1088–1100.

Grammer, T.C., Khokha, M.K., Lane, M.A., Lam, K., and Harland, R.M. (2005). Identification of mutants in inbred *Xenopus tropicalis*. Mech. Dev. *122*, 263–272.

Hachet, V., Köcher, T., Wilm, M., and Mattaj, I.W. (2004). Importin alpha associates with membranes and participates in nuclear envelope assembly in vitro. EMBO J. *23*, 1526–1535.

Hall, M.N., Raff, M.C., and Thomas, G. (2004). Cell growth: control of cell size (Cold Spring Harbor, N.Y.: Cold Spring Harbor Laboratory Press).

Heald, R., and McKeon, F. (1990). Mutations of phosphorylation sites in lamin A that prevent nuclear lamina disassembly in mitosis. Cell *61*, 579–589.

Heitlinger, E., Peter, M., Häner, M., Lustig, A., Aebi, U., and Nigg, E.A. (1991). Expression of chicken lamin B2 in *Escherichia coli*: characterization of its structure, assembly, and molecular interactions. J. Cell Biol. *113*, 485–495.

Horner, H.A., and Macgregor, H.C. (1983). C value and cell volume: their significance in the evolution and development of amphibians. J. Cell Sci. *63*, 135–146.

Jenkins, H., Hölman, T., Lyon, C., Lane, B., Stick, R., and Hutchison, C. (1993). Nuclei that lack a lamina accumulate karyophilic proteins and assemble a nuclear matrix. J. Cell Sci. *106*, 275–285.

Jorgensen, P., Edgington, N.P., Schneider, B.L., Rupes, I., Tyers, M., and Futcher, B. (2007). The size of the nucleus increases as yeast cells grow. Mol. Biol. Cell *18*, 3523–3532.

Lemaitre, J.M., Géraud, G., and Méchali, M. (1998). Dynamics of the genome during early *Xenopus laevis* development: karyomeres as independent units of replication. J. Cell Biol. *142*, 1159–1166.

Loewinger, L., and McKeon, F. (1988). Mutations in the nuclear lamin proteins resulting in their aberrant assembly in the cytoplasm. EMBO J. *7*, 2301–2309.

Lowe, A.R., Siegel, J.J., Kalab, P., Siu, M., Weis, K., and Liphardt, J.T. (2010). Selectivity mechanism of the nuclear pore complex characterized by single cargo tracking. Nature, in press. Published online September 1, 2010. 10.1038/nature09285.

Madrid, A.S., and Weis, K. (2006). Nuclear transport is becoming crystal clear. Chromosoma *115*, 98–109.

Manor, U., and Kachar, B. (2008). Dynamic length regulation of sensory stereocilia. Semin. Cell Dev. Biol. *19*, 502–510.

Maresca, T.J., and Heald, R. (2006). Methods for studying spindle assembly and chromosome condensation in *Xenopus* egg extracts. Methods Mol. Biol. *322*, 459–474.

Marshall, W. (2002). Size control in dynamic organelles. Trends Cell Biol. *12*, 414–419.

Marshall, W.F. (2008). Engineering design principles for organelle size control systems. Semin. Cell Dev. Biol. *19*, 520–524.

Maul, G.G., and Deaven, L. (1977). Quantitative determination of nuclear pore complexes in cycling cells with differing DNA content. J. Cell Biol. *73*, 748–760.

Montorzi, M., Burgos, M.H., and Falchuk, K.H. (2000). *Xenopus laevis* embryo development: arrest of epidermal cell differentiation by the chelating agent 1,10-phenanthroline. Mol. Reprod. Dev. *55*, 75–82.

Murray, A.W. (1991). Cell cycle extracts. Methods Cell Biol. *36*, 581–605.

Neumann, F.R., and Nurse, P. (2007). Nuclear size control in fission yeast. J. Cell Biol. *179*, 593–600.

Newport, J.W., Wilson, K.L., and Dunphy, W.G. (1990). A lamin-independent pathway for nuclear envelope assembly. J. Cell Biol. *111*, 2247–2259.

Nieuwkoop, P.D., and Faber, J. (1967). Normal table of *Xenopus laevis*, Second Edition (Amsterdam: North-Holland Publishing Company).

Prüfert, K., Vogel, A., and Krohne, G. (2004). The lamin CxxM motif promotes nuclear membrane growth. J. Cell Sci. *117*, 6105–6116.

Riddick, G., and Macara, I.G. (2005). A systems analysis of importin-alpha-beta mediated nuclear protein import. J. Cell Biol. *168*, 1027–1038.

Riddick, G., and Macara, I.G. (2007). The adapter importin-alpha provides flexible control of nuclear import at the expense of efficiency. Mol. Syst. Biol. *3*, 118.

Sive, H.L., Grainger, R.M., and Harland, R.M. (2000). Early development of *Xenopus laevis*: a laboratory manual (Cold Spring Harbor, N.Y.: Cold Spring Harbor Laboratory Press).

Smith, A., Brownawell, A., and Macara, I.G. (1998). Nuclear import of Ran is mediated by the transport factor NTF2. Curr. Biol. *8*, 1403–1406.

Smith, A.E., Slepchenko, B.M., Schaff, J.C., Loew, L.M., and Macara, I.G. (2002). Systems analysis of Ran transport. Science *295*, 488–491.

Stewart, M. (2007). Molecular mechanism of the nuclear protein import cycle. Nat. Rev. Mol. Cell Biol. *8*, 195–208.

Theerthagiri, G., Eisenhardt, N., Schwarz, H., and Antonin, W. (2010). The nucleoporin Nup188 controls passage of membrane proteins across the nuclear pore complex. J. Cell Biol. *189*, 1129–1142.

Webster, M., Witkin, K.L., and Cohen-Fix, O. (2009). Sizing up the nucleus: nuclear shape, size and nuclear-envelope assembly. J. Cell Sci. *122*, 1477–1486.

Wilson, N.F., Iyer, J.K., Buchheim, J.A., and Meek, W. (2008). Regulation of flagellar length in *Chlamydomonas*. Semin. Cell Dev. Biol. *19*, 494–501.

Zink, D., Fischer, A.H., and Nickerson, J.A. (2004). Nuclear structure in cancer cells. Nat. Rev. Cancer *4*, 677–687.